Prompting droplet breakup by imposing an electric field

Ningguang Chen(陈宁光),[1] Yunhua Gan(甘云华),[1,a)], and Yuying Yan(阎玉英)[2]

AFFILIATIONS

[1]School of Electric Power Engineering, South China University of Technology, Guangzhou 510640, P.R. China

[2]Faculty of Engineering, University of Nottingham, University Park, Nottingham, UK

[a)]**Author to whom correspondence should be addressed:** ganyh@scut.edu.cn

ABSTRACT

Various means for manipulating droplets based on pressure, magnetic, optical, or other external fields have emerged. Despite the remarkable progress, the existing modalities of droplet formation control and manipulation still deserve further investigations, especially for the utilization of biodiesel. Here, we report a method for droplet manipulation using electric fields to achieve improved uniformity of droplet distribution, continuity and stability of droplet generation. Leveraging on the weakening of surface tension by electric stress could manipulate the droplet size, generation period, and departure rate. When the applied voltage is of 4kV, the droplet size and formation time were reduced by 50% and 7.83 times, respectively. Furthermore, we utilized ethanol with lower surface tension and higher electrical conductivity to improve the response of biodiesel to the electric field, which reduced the droplet breakup time by 211.67 times. Among them, the electric field had the most significant effect on promoting the breakup of BE10 fuel. In addition, the effects of electrode structure and fuel flow rate on droplet breakup in the electric field are also considered. These findings provide a satisfactory paradigm for droplet operation in various practical applications.

I. INTRODUCTION

As a renewable energy source, the emission characteristics and environmental friendliness of biodiesel determine its potential application in the combustion field[1-4]. However, high viscosity means poor flowability, making it difficult to achieve the desired atomization effect and engine performance[5, 6]. Therefore, various external stimuli including electricity[7-9], magnetism[10, 11], and light[12, 13] are introduced to achieve more flexible and precise manipulation in the droplet formation to ensure adequate atomization performance of the fuel.

For a neutral liquid, the breakup mechanism has been well developed since the instability was first considered by Rayleigh[14]. In general, the formation of droplets is associated with inertial forces, gravitational forces, capillary forces, and viscosity effects[15-18]. However, the presence of an electric field plays a key role in influencing droplet formation[19]. For electric based manipulation, the droplet formation occurs primarily through the distribution of charge on the liquid surface resulting in electrical stress overcoming surface tension[20-23]. Droplets carrying the same charges are rapidly driven by Coulomb repulsion to avoid coalescence between droplets. Adjusting the appropriate electric field, the distribution of droplets is characterized by good monodispersity[24, 25]. Therefore, a few works were conducted to explore the effect of electric fields on the morphology of electrospray by carrying out experimental and numerical studies[17, 26]. The results all indicated that electric fields are uniquely suited to control droplet generation and spray transformation[25, 27].

Moreover, the response of droplet formation to the electric field varies with the fluid properties. The low electrical conductivity of biodiesel hints at the difficulty of electric-based manipulation. It can be solved by the addition of higher conductivity fuels with less viscous and lower surface tension into the biodiesel to achieve

improved electrospray characteristics of biodiesel[28-30]. Classical additives reported in recent years include butanol, alcohol, n-pentanol, and ethanol[30, 31]. The results found that blending ethanol can most effectively reduce the emissions of particulate matter and NO_X while achieving optimized atomization performance. The adjustment of the blending ratio optimizes the physical properties of biodiesel to varying degrees, which will have different effects on the droplet formation in the electric field.

Alternatively, electrode structures change the strength of electric field at the capillary exit may provide a promising avenue for droplet generation manipulation[32, 33]. The cone-jet was studied by using a novel capillary with an external electrode[34] and a curved ground electrode[35]. In addition, the electrospray modes were also obtained by double capillaries and multi-nozzle, and the influence of tubes on spray was discussed[36, 37]. It has been demonstrated that the electrode structure significantly affects the electrospray, but studies on the droplet formation are still lacking. Therefore, it is necessary to carry out the study of charged droplet breakup by replacing different electrodes.

Previous studies have proved that the applied voltages, properties of liquid, electrode structure, and flow rate are the key factors in determining the droplet formation mode. In the present work, electric stress is employed to assist droplet formation. The physical properties of the fuel, the electrode structure, and the flow rate are fully considered. Firstly, we prepared blended fuels by adding different ratios of ethanol to biodiesel. The optimized effects of different blended fuels relative to pure biodiesel on droplet formation in the electric field were compared to determine the optimal blending ratio for the electric response by evaluating the droplet formation period, droplet size, stability and continuity of droplet formation, uniformity of the droplet size distribution, and the departure velocity of the droplets. In addition, the

kinetic behavior of the optimally blended fuel and the interaction of the charged droplets in an electric field was further investigated by adjusting capillary specification and flow rate.

II. EXPERIMENTAL DESCRIPTION AND FABRICATION OF FUELS

A. Experimental setup

Figures 1(a) and 1(b) show the experimental setup of droplet formation during an electrospraying process, which comprises an electrostatic generation system, a fuel supply system, and an imaging system. In the electrostatic generation, the capillary is connected to the positive of high voltage electrostatic generation (HVEG) (BOHER HV, 71230P, China), and the range of applied voltages is from 0 kV to 8 kV. The negative of the HVEG is connected to the grounding mesh. The set of the capillary is shown in Fig. 1(c). The distance of H can be calculated as follows:

$$H = H_1 - (H_2 - H_4) \tag{1}$$

$$H_4 = H_3 \frac{L_3 - L_1}{L_3 - L_2} \tag{2}$$

The parameters of H_1, H_2, H_3, L_1, L_2, and L_3 can be found in Fig. 1(c). Therefore, the distance of H is 21.75 mm. A micro syringe pump (ISPLab02, China) is used in this study as the fuel supply system. The flow rate of fuel ranges from 10 ml/h to 50 ml/h. The Fuel is pumped into a metal capillary at a set flow rate, and broken into droplets with different sizes in an electric field. The imaging system comprises a high-speed camera (Phantom VEO, 1310L, USA), a light source, and a computer. The high-speed camera is employed to capture behaviors of droplet formation and motion in the electric field. The resolution of the high-speed camera is set to 1280×804 with a frame rate of 3000 fps, which means that 3,000 consecutive pictures could be taken

per second. The light source is set in backlight mode, and a piece of scattering film is employed to evenly distribute the light source.

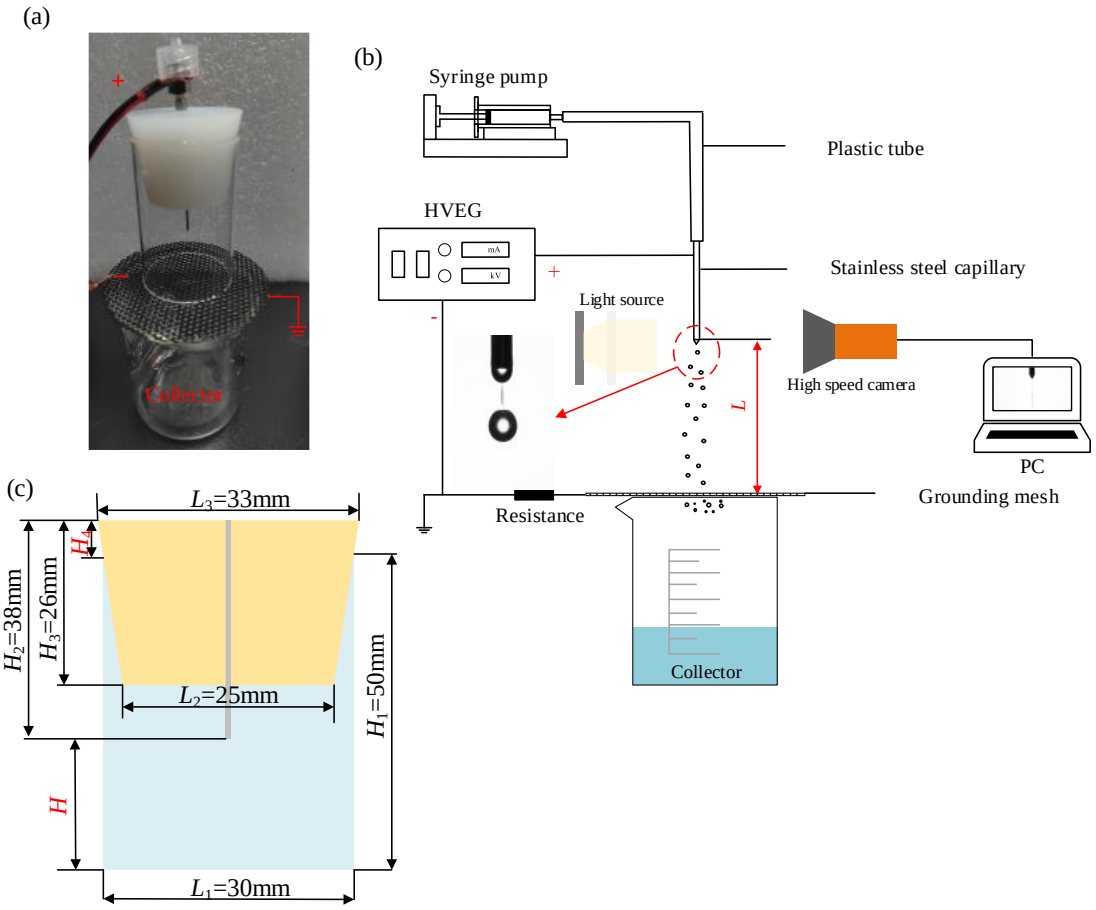

FIG. 1. Schematic of the experimental setup of the electrospray system. (a) The picture of the experimental setup. (b) The Schematic drawing of the droplet formation during the electrospraying process. (c) The set of the distance between the exit of capillary and grounded mesh.

B. Fabrication of fuels

As a renewable energy source, the good emission characteristics and environmental friendliness of biodiesel determine its potential application in the combustion field. However, the high viscosity and low electrical conductivity mean that it has poor fluidity and electro-atomization, which affects the engine performance. The conductivity and fluidity of ethanol are much better than that of biodiesel, and there is a good compatibility between ethanol and biodiesel. To obtain fuels with different physical properties, we first add different volume ratios of ethanol

to biodiesel. The ratio of biodiesel to ethanol B: E is 90:10, 80:20, 70:30, 60:40, and 50:50, respectively. The mutual solubility of the two fuels in different blending ratios was tested at 25℃ and no separated layer was found after standing for 5 days, and the properties of the test fuels are shown in Table I.

TABLE I Compositions and properties of the test fuels. (298 K).

Test fuels	B100	BE10	BE20	BE30	BE40	BE50
Ethanol (% by volume)	0	10	20	30	40	50
Biodiesel (% by volume)	100	90	80	70	60	50
Dynamic viscosity μ (mPa·s)	6.05	4.64	3.68	3.22	2.67	2.48
Surface tension σ (N/m)	0.034	0.033	0.031	0.029	0.027	0.026
Electrical conductivity K (S/m)	5.0E-10	4.7E-9	3.5E-8	8.7E-7	5.2E-6	7.9E-5
Density ρ (kg/m^3)	870	860	852	846	838	830

III. RESULTS AND DISCUSSION

A. Droplet formation of biodiesel affected by electric field

The droplet formation of biodiesel is a key issue to optimize the combustion process. To study the formation of droplets promoted by an electric field, we used a syringe pump to continuously supply biodiesel with a flow rate of 10 ml/h. The specification of the capillary is selected as 20G (outer diameter is 0.9 mm, and the inner diameter is 0.6 mm), which can produce droplets with a diameter of ~2.56 mm under neutral conditions. Biodiesel will be broken and move in the electric field traction formed between the metal capillary and the grounded grid. The schematic drawing of the droplet formation during the electrospraying process is provided in Fig. 2(a). Figure. 2(b) shows the typical observed behavior of droplet formation in the absence of an electric field. The ending of the previous droplet breakup is the beginning of the present droplet formation. Once the previous droplet separates from the capillary, the increase of surface energy causes the phase interface at the front end

of the pinhole to shrink, lasting for approximately 3 ms. As a result, any excess kinetic energy is dissipated through the interface oscillation during the shrink process[38]. Under the promotion of the capillary effect, the liquid interface will continue to climb upwards along the capillary by ~2.43 mm with a contact angle of 26.57° between biodiesel and the capillary. The expansion stage of the droplet would last for 2.81 s, accounting for 89.78% of the total droplet formation time. The droplet develops rapidly in a spherical shape owing to the continuous injection of biodiesel. The droplet would undergo irreversible stretching and fracture (~3.13 s), when the contact angle between the interface and capillary exit reaches 90°. Note that the stretching stage lasted for 0.317 s, accounting for 10.13% of the total droplet formation time. At this point, an independent droplet is formed and leaves at a speed of 0.2 m/s.

In comparison, the application of electric field reduces the surface energy of the droplet, due to the increase of accumulated charges[39]. According to the surface energy minimization principle, the molecular forces on the interface would be weakened, making droplets more susceptible to deformation and fragmentation when subjected to external forces[15, 40]. Once the charge density exceeds the Rayleigh limit[41] ($q_{\text{Rayleigh}} = 2\pi\sqrt{2\varepsilon_0\sigma D^3}$, where ε_0 and σ denote the permittivity of vacuum and the surface tension of the droplet), the droplet breaks to release charges. Therefore, the participation of electric fields increases the frequency of droplet formation while also reducing droplet size. Higher applied voltages (2 kV, 3 kV, 4 kV) led to the creation of smaller droplets, which reduced the diameter of the droplet from 2.56 mm (V = 0 kV) to 1.31 mm (V = 4 kV), as shown in Fig. 2(c) to 2(e). The period of interface shrinkage always remains at 3 ms, while the expansion phase rapidly decreases from 2.81 s (V = 0 kV) to 0.34 s (V = 4 kV). Especially, when the applied voltage is of 4

kV, the droplet will no longer climb up along the metal capillary affected by the capillary effect. Compared to neutral droplets, the formation time was shortened by 7.83 times when the applied voltage was 4 kV. The shortening of the droplet formation period is mainly due to the contribution of the expansion stage, which has decreased by 8.26 times.

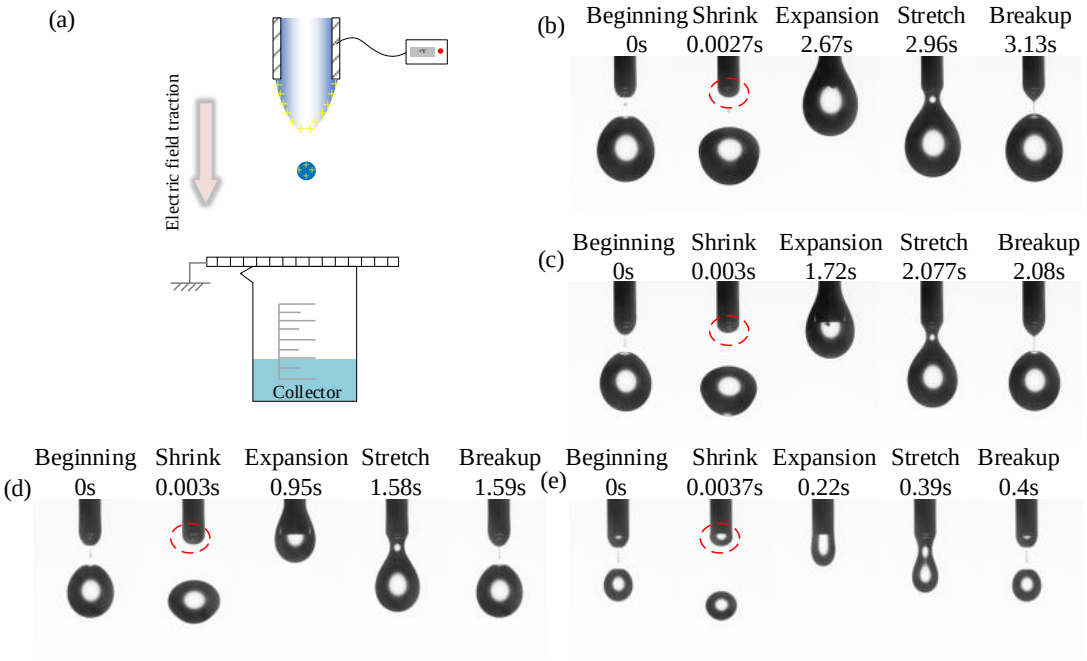

FIG. 2. Droplet formation of biodiesel affected by the electric field. (a) Schematic drawing of the droplet formation platform. (b) A droplet expands at the outlet of the capillary and lasts for 2.81s (V = 0 kV). (c) A droplet expands at the outlet of the capillary and lasts for 1.95s (V = 2 kV). (d) A biodiesel droplet expands at the outlet of the capillary and lasts for 1.49s (V = 3kV). (e) A droplet expands at the outlet of the capillary and lasts for 0.34s (V = 4kV).

With the increase in applied voltages, the diameter of the departure droplet will be further reduced due to the increase in charge density ($q \sim \nabla \cdot (\varepsilon E)$) on the droplet surface. As shown in Fig. 3(a), an applied voltage of less than 6 kV means that the system always produces single droplets with larger sizes. When the voltage reaches 6 kV, the incoming flow will emit several small droplets (with sizes as small as tens of

micrometers) to achieve the purpose of releasing charges. However, under the action of hydrodynamics, a larger unstable droplet (D~0.8 mm) will still follow closely. The movement speed of fine droplets in an electric field can reach 3 m/s, which is far exceeding that of neutral droplets (0.2 m/s), benefiting from the increase in Coulomb repulsion and the reduction of droplet size. In addition, the cone height decreases with the increase of voltage. When the voltage is 8 kV, the cone height is 1.25 mm, which is 37.81% lower than that at V = 7 kV.

In the absence of an electric field, the droplets are mainly formed in a quasi-static form at the nozzle by gravity overcoming surface tension, as shown in Fig. 3(b). In theory, the diameter of the formed droplets is 2.43 mm ($D \sim (6d_{in}\sigma/\rho g)^{1/3}$, where d_{in} is the inner diameter of the capillary, σ denotes the surface tension, ρ is the density of the liquid, and g is the gravitational acceleration)[41]. In our experimental measurements, the diameter of the neutral droplet is 5% larger than the theoretical value. The presence of an electric field has two main roles at the interface[42], as shown in Fig. 3(c). On the one hand, the electric stress overcomes the surface tension of the droplet ($\sigma_e \sim \sigma - q^2/(8\pi^2\varepsilon D^3)$)[43] and promotes droplet formation. As a result, the droplet size is reduced by the self-repulsion of the free charges. On the other hand, the electric polarization stress generated by the permittivity gradient between the liquid and gas prevents the local electric field from shrinking and promotes the movement of droplets from strong fields to weak fields[44]. According to the discussion on the direction of the acting forces by Zhang[42, 45], the electric field at the liquid-gas interface can be decomposed as normal and tangential components, which is shown in Fig. 3(d).

In general, the complete formation of droplets is simplified as three stages, including shrinking after the departure of the previous droplet, the expansion of the current droplet, and the narrowing of the liquid bridge caused by stretching of the droplet, which is depicted in Fig. 2(b) to 2(e). The stretching plays a key role in the formation of droplets. When the voltage is applied, the distribution of the charges on the interface could be simplified and indicated in Fig. 3(e). The configuration of the liquid bridge undergoes deformation, which results from the synergistic effect of tangential electric stress (stretching the droplet) and inertial force. Therefore, the liquid bridge becomes narrower and narrower until the liquid film separates and the droplets are completely broken. Notably, increasing applied voltage considerably shortens the duration of the shrinkage of the liquid bridge, which also leads to a further reduction in droplet volume under a high-voltage system. The broken droplets are accelerated away by Coulomb repulsion ($F \sim qE$) due to carrying charges with the same polarity.

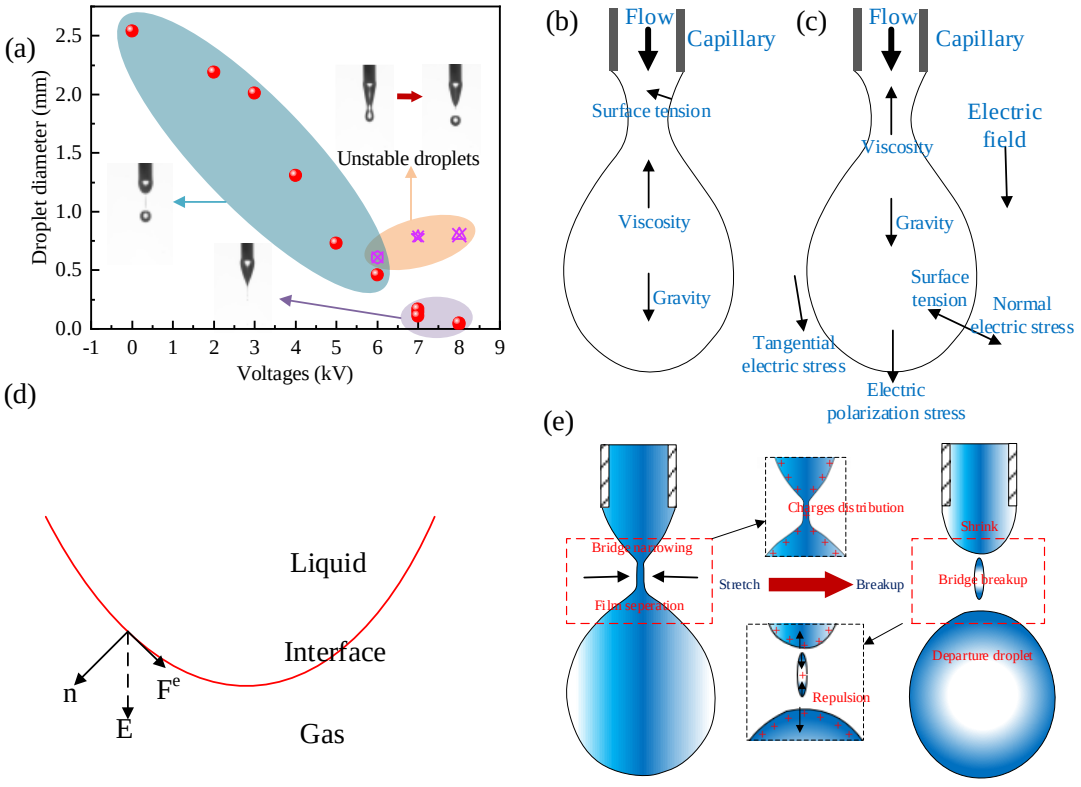

FIG. 3. The diameter of the droplets varies with the applied voltages (a) Droplet diameter of biodiesel under various electric fields. (b) Schematic of the droplet formation mechanisms of neutral liquid. (c) Forces acting on a growing droplet under the electric field. (d) A normal (n) and a tangential (F^e) component decomposed from the electric field on the interface. (e) Simplified droplet breakup in an electric field and its charge distribution and transportation.

B. Droplet characteristics

The physical property of biodiesel is one of the important considerations for prompting droplet breakup by imposing an electric field. The prerequisite for the accumulation of free charges on the surface of droplets is that the speed of charge movement is greater than the fluid flow rate. The droplet breakup occurs when the local charge density exceeds a critical value[46]. However, biodiesel exhibits poor electrospray performance due to a larger charge relaxation time[47] ($\tau_e \sim \varepsilon/K$, the conductivity of biodiesel is 5×10^{-10} S/m). Considering the good electrospray performance of ethanol (the conductivity K~5×10^{-5} S/m), blending it to biodiesel is an effective way to improve the quality of electrospray. Without considering the electric field assistance, the droplet size of BE50 is reduced by 8% compared to B100 and differs from the theoretical value ($D \sim (6d_{\text{in}}\sigma/\rho g)^{1/3}$) by 4%. In addition, the contact angle for the mixture and the capillary was reduced by 47.16% as shown in Table II, which is mainly due to the reduction of surface tension. Figure. 4(a) shows the image capture of droplets generated by different blended fuels. In addition, the period of droplet formation is shortened by 18.85%, which is attributed to the reduction of the hydrodynamic relaxation time ($\tau_h \sim \mu r_{\text{in}}/\sigma$, which denotes the mechanical deformation velocity of the capillary waves). By applying a voltage to the experimental system, we found that fuels with different blending ratios respond

differently to the electric field due to changes in physical properties. As shown in Fig. 4(b), the droplets generated by BE10 show good uniformity and continuity.

TABLE II. **The contact angle for the mixture and the capillary.**

Test fuels	B100	BE10	BE20	BE30	BE40	BE50
Contact angle	26.57°	23.63°	21.62°	19.09°	17.35°	14.04°

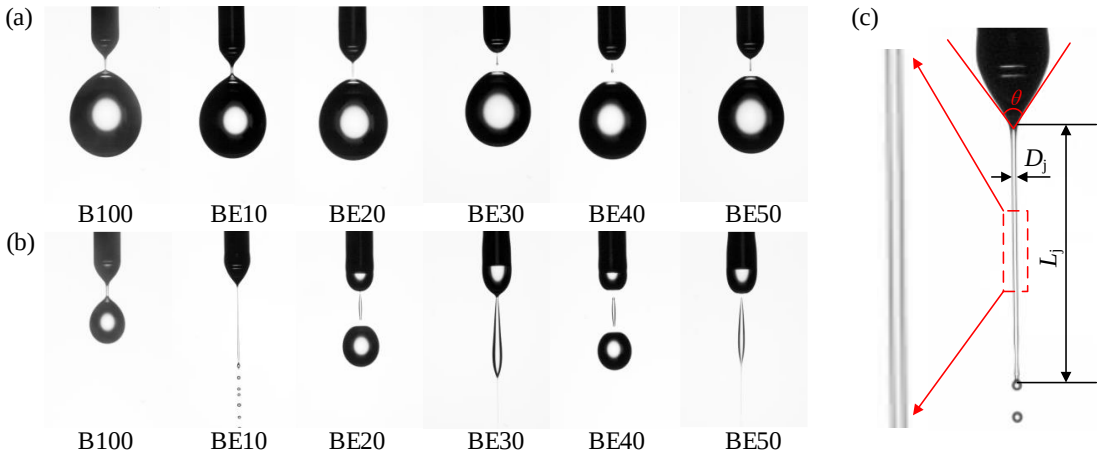

FIG. 4. Comparison of droplet formation of different blending ratios under the electric field (Q=10ml/h). (a) Image capture of droplets generated by different blended fuels (V=0). (b) Image capture of droplets generated by different blended fuels(V=4kV). (c) The structure of jet.

When the applied voltage is V = 4 kV, a spiral jet with a diameter of 0.06 mm and a length of 3.52 mm will be ejected from the conical tip again every 7.33 ms, as shown in Fig. 4(c). When the cone angle θ is less than 54.46°, fine droplets start to form, and then the whole jet breaks up and fragments into several small droplets with a diameter of 0.14 mm, which are moving toward the grounded electrode with a speed of 2.2 m/s. Compared to the rest of the blending ratio fuels, BE10 exhibits better electrical response characteristics in an electric field environment, specifically reflected in the ability to generate finer droplets, faster droplet movement speed, and more stable generation. In addition, BE20 and BE40 fuels respond much less well to electric fields. Droplets comparable to biodiesel were still produced at 4 kV. However,

the droplet fragmentation modes of BE30 and BE50 are similar, both in spindle mode. A series of fine droplets with a diameter of several tens of micrometers are ejected from the tip of the spindle, and then the spindle-shaped droplets move in an electric field at a speed of 0.9 m/s and undergo morphological changes. Similarly, the cone angle θ when ejecting droplets from cone tips with different blending ratios is similar at about 55°. Overall, the BE10 showed a more sensitive response to the electric field and could stably produce uniform clusters of fine droplets.

Furthermore, we control the applied voltage to probe the droplet formation modes for fuels with different blending ratios. The experimental results show that the fuels with different blending ratios exhibit dramatically different responses to electric fields. Figure 5 depicts the image capture of droplets generated by different blended fuels in various electric fields. BE10 demonstrated outstanding electrospray performance, especially at a voltage of 5 kV. A stable cone angle θ (69.42°) was formed at the exit of the capillary and a jet with a length of 1.48 mm was maintained at the tip of the cone. Droplets with a size of 45 μm and a spacing of 0.35 mm were continuously generated at the tip of the jet and moved toward the grounded electrode at a speed of 3.08 m/s. The stable characteristics of droplet formation show that the electric effect is far greater than the inertial force, and the electric force dominates the droplet formation process. The increase in voltage means that the charge density on the droplet surface is more likely to reach the critical value[48] (Rayleigh limit, $q_{\text{Rayleigh}} \sim 2\pi\sqrt{2\varepsilon_0\sigma D^3}$), and the greater Coulomb repulsion leads to an increase in droplet velocity. By further increasing the voltage, the surface disturbance of the liquid at the outlet of the capillary is enhanced, leading to the selective accumulation of charges in several local areas and the first to reach the Rayleigh limit, which results in multiple jets. The number of jet streams will be positively correlated with the

electric field. In addition, the spray range will also be expanded as the voltage increases. The spray range θ_r, represented by the atomization cone angle, will increase from 70.7° at 6 kV to 91.34° at 8 kV.

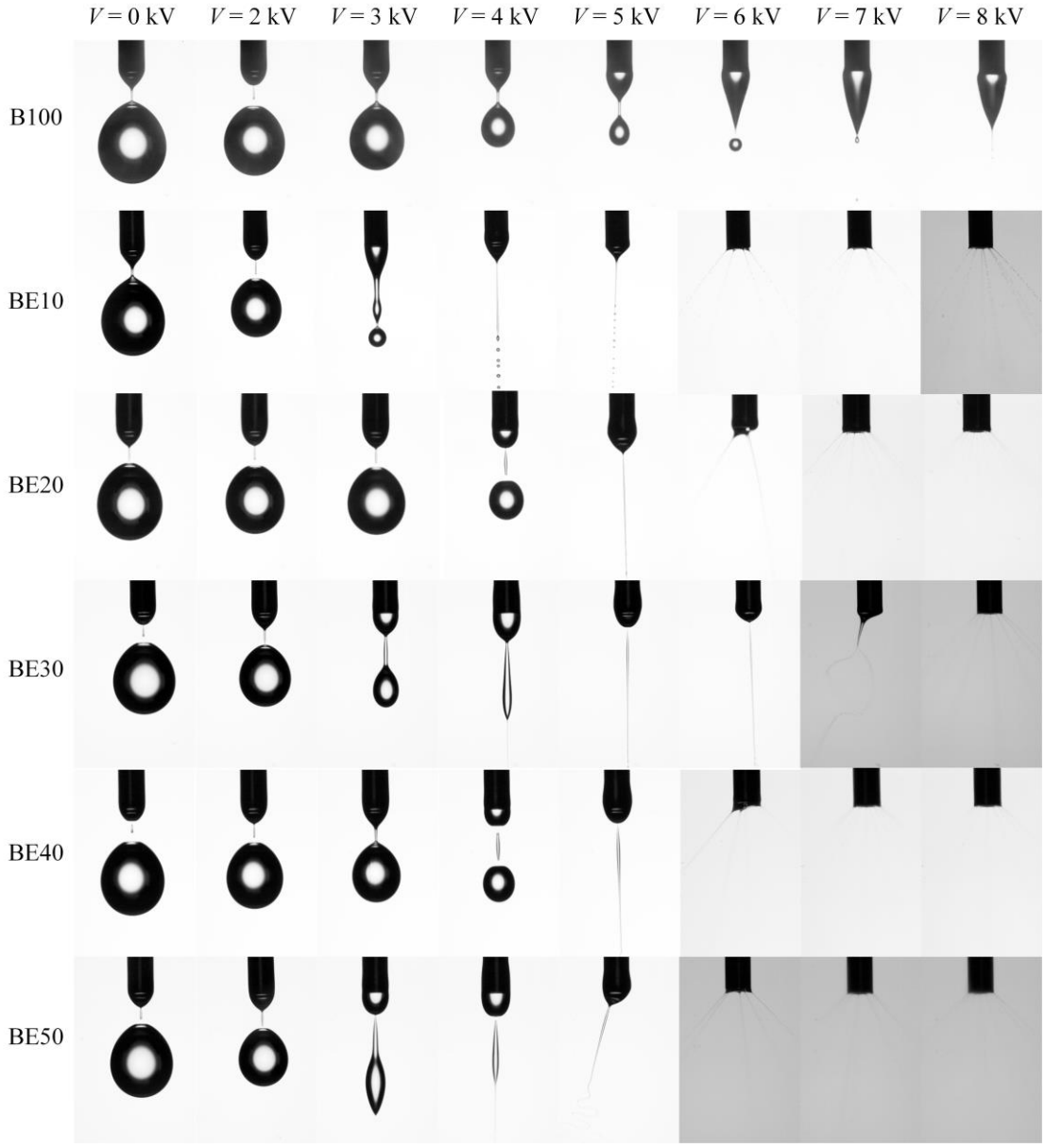

FIG. 5. Image capture of droplets generated with different blended fuels in various electric fields. Fuel is injected into the metal capillary at a flow rate of 10ml/h.

Comparing the response of fuels with different blending ratios to the electric field, we statistically characterize the droplet formation modes, as shown in Fig. 6(a). As the increase of blending ratio and voltage, the droplet formation modes will go

through dripping, stable jet, spindle, unstable jet, and stable multi-jet sequentially. The droplet formation mode of biodiesel in different electric fields is dominated by dripping due to the smaller conductivity (K~5×10^{-10} S/m). In terms of droplet formation mode distribution, BE10 can be proven to be the most stable blending ratio for droplet formation in an electric field.

The size of the droplet is one of the important parameters to measure the degree of fuel fragmentation. We have counted the variation of average size with voltage for different blended fuels, which can be illustrated in Fig. 6(b). The charge density of droplets increases with increasing voltage, resulting in a decrease in the average droplet size. The average diameter of droplets produced by BE10 fuel in an electric field is the finest. When the electric field force is not enough to weaken the surface tension (V < 4 kV), the droplets will be dominated by inertial forces to produce larger droplets. However, when the voltage is greater than 4 kV, it can be observed that the blended fuel is well fragmented into fine droplets at the micrometer level. Biodiesel still drops larger droplets due to the competition between electric field force and surface tension caused by the large electrical relaxation time unfavorable to free-charge transport. Therefore, blending a certain percentage of ethanol in biodiesel can effectively improve the electrospray effect of the fuel. Compared with biodiesel, BE10 has the best degree of fragmentation in the electric field. The effect was gradually significant when the voltage was greater than 3 kV, and the average particle size could be reduced by a maximum of 18.4 times (V = 6 kV). In addition, compared to the absence of an electric field, the boosting of electric stress can significantly reduce the droplet size, especially the response of BE10 to the electric field. The droplet size decreases with increasing electric field up to 211.67 times (V = 8 kV),

while the droplet size of biodiesel decreases only up to 64 times, as shown in Fig. 6(c).

The departure velocity is an important parameter to characterize droplet motion. The charged droplet is mainly accelerated by the electric field force ($F \sim qE$) during its motion. In the shooting field of view, we assume that the droplet is moving at a uniform speed. Figure 6(d) depicts the variation trend of droplet velocity of different blended fuels with applied voltages. As increasing the applied voltages, the departure velocity of droplets is increased, and the maximum velocity can reach 4.2 m/s, which is 17.77 times higher than that in the absence of an electric field. Overall, the droplet velocity of blended fuel is larger than that of biodiesel, and BE10 has the largest motion velocity. In addition, compared to biodiesel, the maximum increase in droplet velocity of BE10 is 4.94 times (V = 4kV). On the one hand, the increase in voltages enhances the charge density on the droplet surface, leading to an increase in Coulomb force. On the other hand, the decrease in droplet size leads to an increase in the acceleration of smaller droplets by the same magnitude of Coulomb force.

The breakup time of the droplets represents the continuity of the electrospray. Since the droplet generation frequency increases with the increase in electric field, we only counted the droplet breakup time for voltages from 0 kV to 6 kV, as shown in Fig. 6(e). Due to the increase in charge density, the droplet breakup time will decrease rapidly as the voltage increases. When the voltage $V \geq$ 4kV, the droplet generation time stabilizes at the millisecond level because the droplet breakup is transformed to be dominated by the electric field force. For biodiesel, the presence of the electric field increases the number of droplets per second by a factor of 90.38 (0kV-6kV). While for BE30, the droplet breakup time is reduced by a factor of 682.17 for the same voltage range. Since ethanol blending reduces the electrical relaxation time τ_e

and accelerates the charge transport, the fragmentation time of the blended fuel is further reduced.

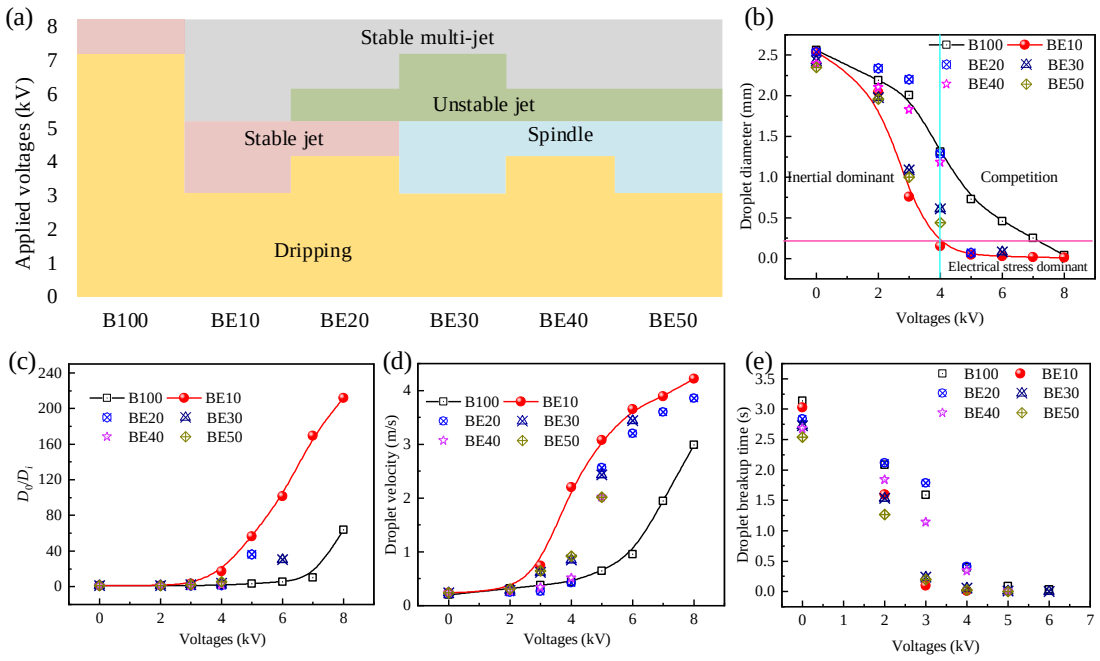

FIG. 6. Comparison of droplet characteristics of different blending ratios under the electric field. (a) Droplet formation modes of fuels with different blending ratios in various electric fields. (b) The variation trend of droplet size of different blended fuels with applied voltages. (c) The degree of fragmentation of different blended fuels in an electric field compared to a neutral environment (Here, D_i, and D_0 are the droplet diameters of any droplet, and droplet at a voltage of 0, respectively). (d) The variation trend of droplet velocity of different blended fuels with applied voltages. (e) The droplet breakup time of different blended fuels under the action of an electric field.

C. Considering capillary diameter and flow rate

Droplet dynamics in an electric field are deeply modified by the capillary specifications. In the experimental system of this study, the flow rate of BE10 fuel was controlled at 10 ml/h through different sizes of capillaries. The outer and inner diameters of the capillary with different specifications are depicted in Table III. Experiments showed that changing the capillary size did not have a significant effect

on the droplet fragmentation process, as shown in Fig. 7(a). Droplets were generated at the exit of different capillaries in a similar mode in the absence of electric field. However, the diameter of the generated droplets decreases with decreasing capillary diameter in the absence of an electric field, as shown in Fig. 7(b). The droplet diameter decreases by 22.14% when replacing G18 with G22 capillary. The difference between the experimental measurement value and the theoretical value ($D \sim (6d_{in}\sigma/\rho g)^{1/3}$) is within 5.39% (G20). With the gradual increase in voltage, dripping, jet, and multi-jet crushing occur sequentially at the exit of different specification capillaries. The jet length is shortened from 4.08 mm in G18 to 1.81 mm in G22 when the voltage is 4 kV, as shown in Fig. 7(a). The electric field strength at the exit of the capillary can be expressed as follows[49]:

$$E = \frac{2V}{r_{out} \ln(4H / r_{out})} \tag{3}$$

where V is the applied voltage, r_{out} is the outer diameter of the capillary, and H is the distance from the exit of the capillary to the grounded electrode. Therefore, the electric field strength at the exit of the capillary is the result of a combination of applied voltage, capillary diameter, and electrode distance. The results found that the electric field strength of G22 is 4.14×10^3 kV/m, which is 59.84% larger than that of G18, as shown in Fig. 7(c). The essence of switching the capillary size is to change the electric field strength at the outlet. The decrease in capillary diameter implies an increase in the electric field strength, which leads to an increase in the charge density on the droplet surface, and thus the jet length is shortened. However, due to the weak electric field strength at the exit, when the voltage is 4 kV, the jets of G18-G20 will break as a whole under the inertial force and then break into several small droplets, while G21 and G22 remain stable with broken jet tips. It means that the voltage for

small-size capillaries to reach a stable jet is decreased. Coincidentally, the cone angle is always about 55° when the droplet breakup mode changes to a jet, as depicted in Fig. 7(d). The continued increase in voltage means that the jet length is shortened and the cone angle is increased.

TABLE III. **The outer and inner diameters of the capillary with different specifications.**

Specification of capillary	G18	G19	G20	G21	G22
Outer diameters (mm)	1.25	1.05	0.9	0.8	0.7
Inner diameters (mm)	0.85	0.7	0.6	0.5	0.4

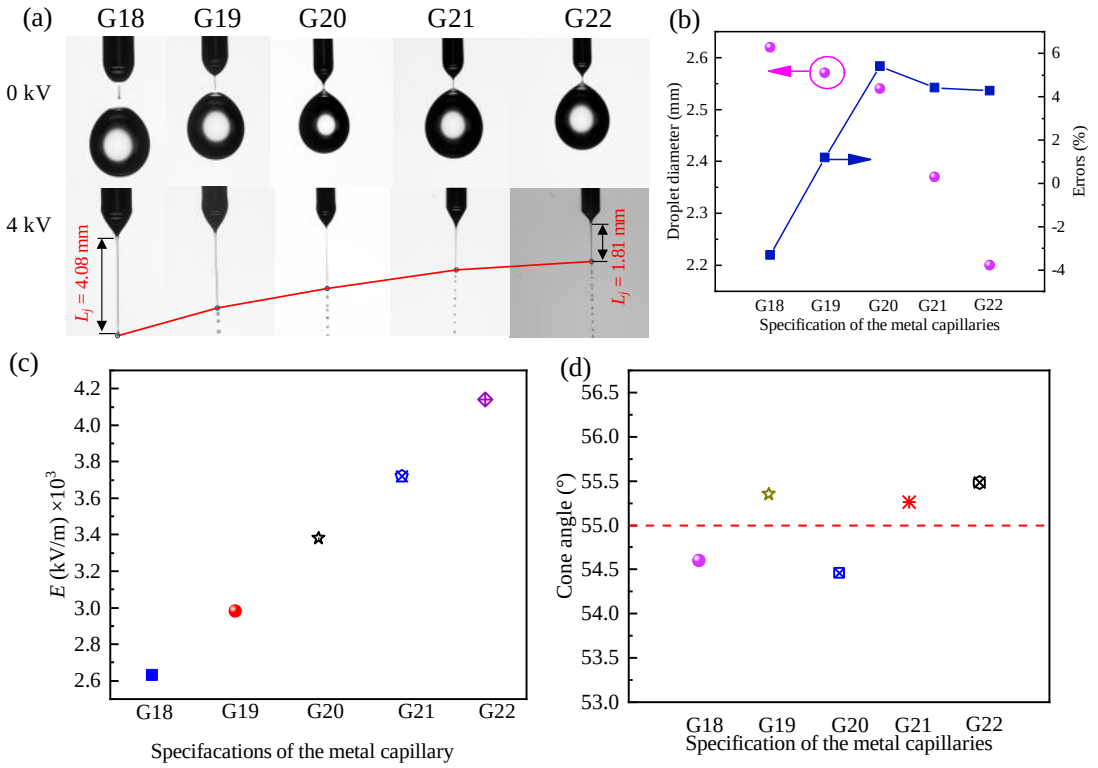

FIG. 7. Droplet formation by considering capillary diameter. (a) Image capture of droplets formation in various capillaries (Q=10 ml/h). (b) The droplet diameter varies with capillaries in the absence of an electric field. (c) Electric field strength at the exit of the capillary. (d) Cone angle when the droplet breakup mode changes to a jet.

During the transition from stable jet mode to multi-jet mode, there is a special stage where the jet tilts along a specific direction (oblique jet), as shown in Fig. 8(a).

The inclination angle θ_j will increase with the decrease in capillary diameter (from 9.3° for G18 to 31.2° for G22). The jet mode will then change to a multi-jet mode. Furthermore, the jet diameter decreases accordingly, implying a decrease in the diameter of the generated droplets[14] ($D \sim 1.89D_j$). The droplet sizes produced by different capillaries show the same trend of response to the electric field, which can be proved in Fig. 8(b). As the droplet fragmentation mode shifted from dripping to jet mode, the droplet size appeared to decrease across scales, rapidly decreasing from the millimeter level to the micrometer level. In addition, the departure velocity of the droplet is also increased by increasing the applied voltage, as shown in Fig. 8(c).

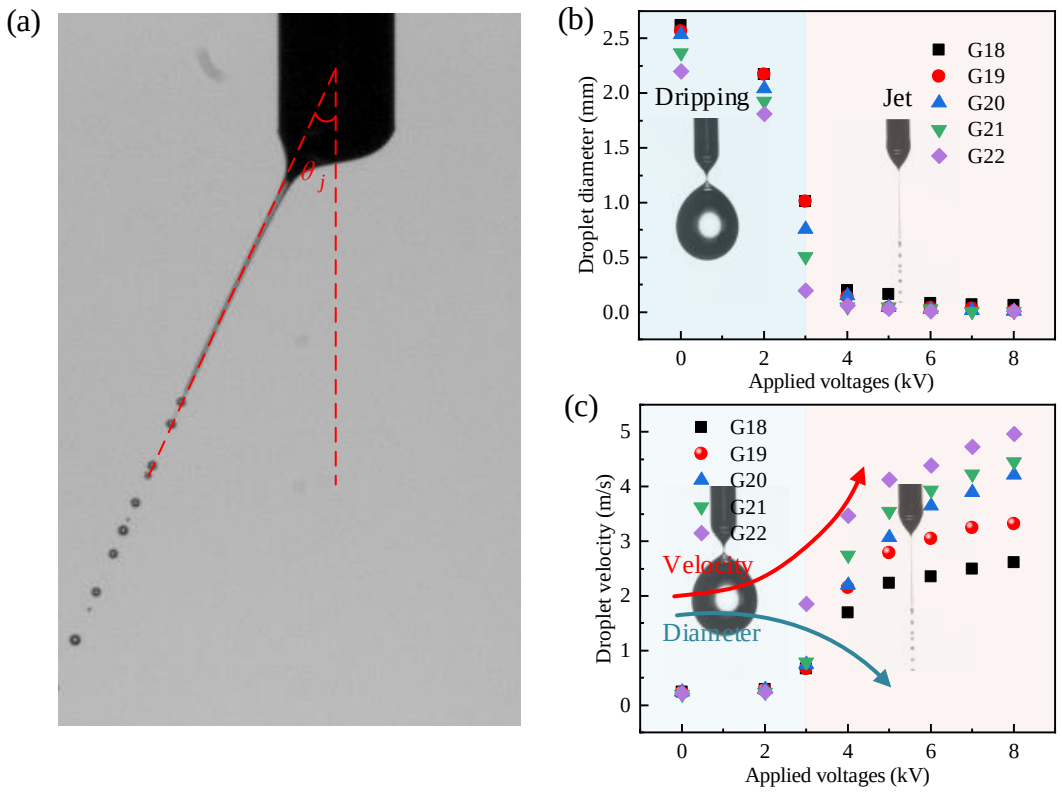

FIG. 8. Droplet characteristics by considering capillary diameter. (a) The inclination angle of the oblique jet. (b) The variation trend of droplet size of different capillaries with applied voltages. (c) The variation trend of droplet velocity of different capillaries with applied voltages.

In addition to capillary size and fuel properties, the flow rate of fuel is also one of the key considerations for combustion optimization. Under conventional

conditions, the jet breakup will be significantly affected by the flow rate of fuel, which is mainly manifested by the weakening of gravity as the flow rate increases, while the gradually dominates the liquid breakup[41]. However, for the charged jet breakup process, the presence of electric field force makes the breakup of droplets under a high flow rate more complicated. Figure. 9 demonstrates the droplet formation of BE10. In the absence of an electric field, droplets are generated by gravity in a dripping mode. The droplet size decreases slightly due to the increased flow rate improving the inertial force. By applying a voltage, the breakup mode of the droplets shifts, which is mainly due to the weakening of the surface tension by the applied voltage. Increasing the fuel flow rate means that the surface charge density at the exit of the capillary decreases, resulting in a weakening of the electric field force and an elevation of the inertial force.

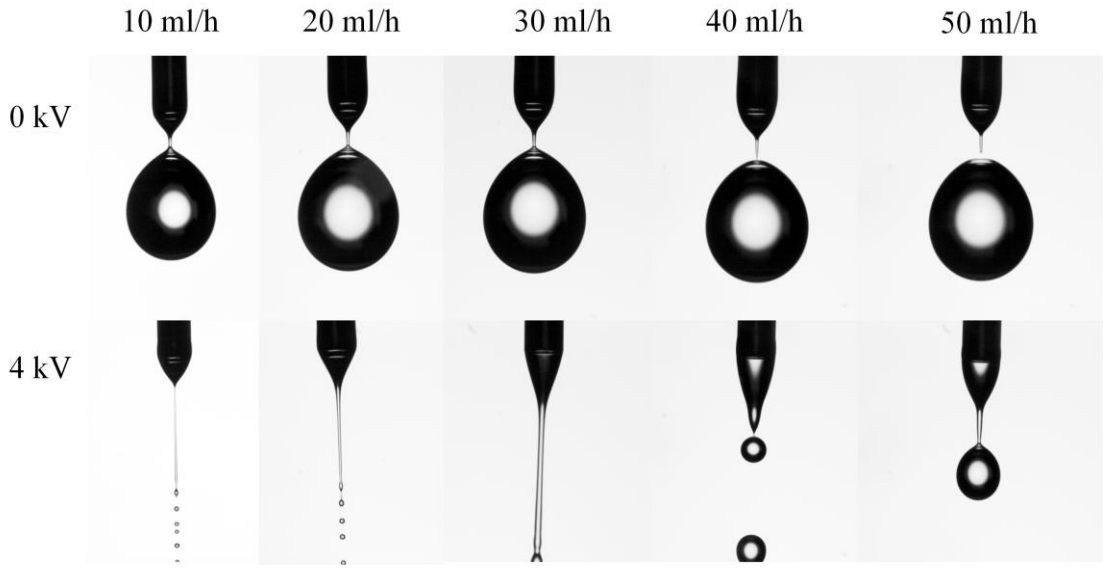

FIG. 9. Image capture of droplets formation various flow rates (G20). A larger flow rate means a greater electric stress is required to fragment the droplets.

When a voltage is applied in this system, the droplets at a flow rate of 10 ml/h are generated in a jet breakup mode with a size of 150 μm and a velocity of 2.2 m/s. However, at a flow rate of 50 ml/h, the droplets were broken in dripping mode to

produce droplets with a diameter of 1.13 mm and a speed of only 0.63 m/s. The droplet diameter increased by 7.53 times under the same voltage condition, which means that increasing the flow rate worsened the droplet breakup. In addition, increasing the flow rate also increases the voltage range for the droplet breakup mode shift.

D. Repulsion between droplets promoted by electric field

The broken droplets move toward the grounded electrode in the electric field by carrying charges of the same polarity. It means that there is interaction between the droplets. To elucidate the mechanism of repulsion between droplets, we revisited the characterization of the motion of charged droplets. Figure. 10 plots the sketch map of repulsion between droplets promoted by an electric field. The density of charges is positively related to droplet volume ($q_{\text{Rayleigh}} \sim 2\pi\sqrt{2\varepsilon_0\sigma D^3}$), which means the strength of the electrical repulsion to which the droplet is subjected. There are two phenomena of repulsion between droplets. First, when the applied voltage is low, the electric stress is not enough to perfectly resist the surface tension and the droplets break up in a larger diameter. In addition, the liquid bridge breaks up into a small droplet with a micrometer size, as shown in Fig. 10(a). Surprisingly, this small droplet does not incorporate into the larger droplet although it moves at a greater speed. Instead, the small droplet is bounced off by the large droplet and reverses its direction of motion when the distance is close. However, the large droplets still move according to the established trajectory, and the repulsive force between the droplets has little effect on them. The shift in the direction of motion of the droplets is mainly due to the fact that the droplets are charged with the same polarity, and the charges migrate when the droplets are close (Fig. 10(b)), changing the motion of the droplets under the action of repulsive forces. Alternatively, when the applied voltage is increased, the

fuel can be sufficiently fragmented to produce droplets with a uniform distribution of droplet size, implying that the droplets are similarly charged. Approaching droplets will simultaneously change their direction of motion under repulsive forces and thus move away again, as shown in Fig. 10(c). The schematic diagram of the interaction between two charged droplets with equivalent volume is shown in Fig. 10(d), the repulsive force has a similar effect on the motion of the two droplets.

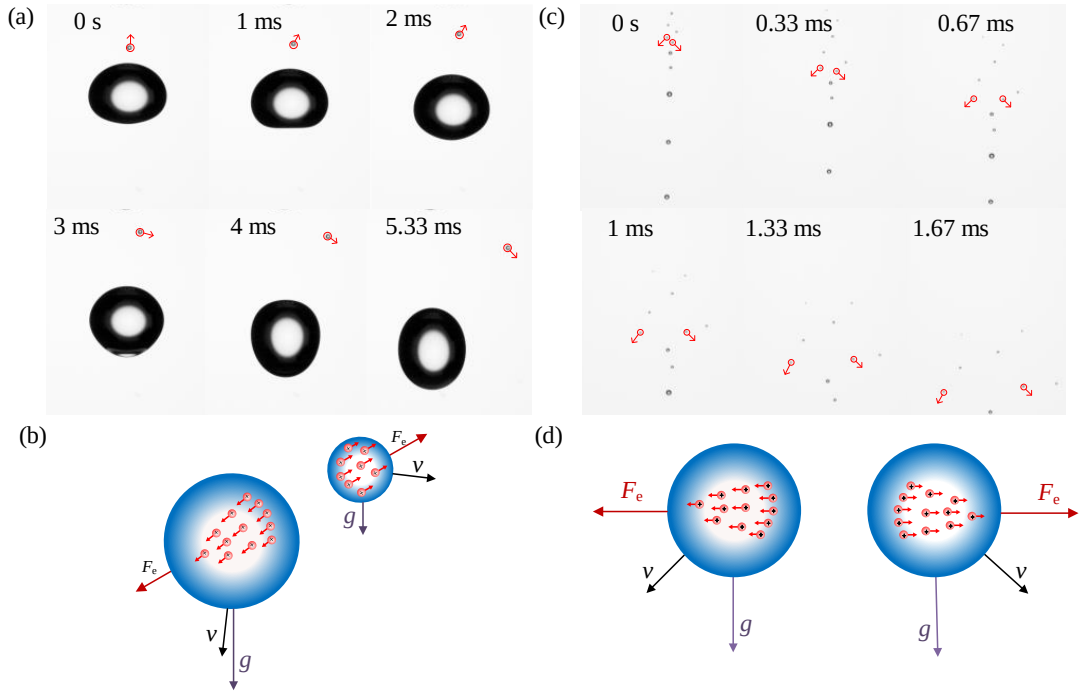

FIG. 10 Repulsion between droplets promoted by the electric field. (a) The motion of two charged droplets with different sizes under Coulomb repulsion. (b) Schematic diagram of the interaction between two charged droplets with different sizes. (c) Two charged droplets with equivalent volume move in opposite directions under the push of Coulomb repulsion. (d) Schematic diagram of the interaction between two charged droplets with equivalent volume.

IV. CONCLUSIONS

In this study, we successfully investigate the formation of droplets promoted by the electric field. The transfer of charges enhances the ability of droplets to undergo Rayleigh breakup, thereby promoting the formation of fine droplets. It was found that

the participation of electric fields increases the frequency of droplet formation by 7.83 times, and reduces droplet size by 50%, which allows us to realize the control of droplet generation and its characteristics of motion by adjusting the strength of the electric field. In addition, the addition of ethanol significantly enhanced the charging performance of biodiesel due to the increase in conductivity. BE10 could obtain the most excellent fragmentation characteristics, which was manifested in the continuous generation of fine droplets with good stability and homogeneity. The change in physical properties decreased the droplet size by 211.67 times. In contrast, changing the capillary diameter and flow rate has a smaller effect on the electric field promoting droplet generation. The change in capillary diameter essentially adjusts the outlet electric field strength, while increasing the flow rate reduces the surface charge density of the droplet. Furthermore, the Coulomb repulsion increases the departure velocity of droplets by 17.77 times in the electric field space and avoids coalescence between droplets. These findings advance the understanding of droplet formation promoted by the electric field and open potential avenues for further exploration of practical applications.

ACKNOWLEDGMENTS

We thank the National Natural Science Foundation of China (52376108), Guangdong Science and Technology Plan (2022A0505050004), and Royal Society (UK) (IEC\NSFC\211210) for generous financial support

AUTHOR DECLARATIONS

Conflict of Interest

The authors have no conflicts to disclose.

AUthor Contributions

Ningguang Chen: Investigation; Writing-original draft. **Yunhua Gan:** Conceptualization; Resources; Funding acquisition; Writing-review & editing; Project administration; Supervision. **Yuying Yan**: Writing-Review & Editing.

DATA AVAILABILITY

The data that support the findings of this study are available from the corresponding author upon reasonable request.

REFERENCES

[1] M. M. Hasan, and M. M. Rahman, "Performance and emission characteristics of biodiesel-diesel blend and environmental and economic impacts of biodiesel production: A review," Renew Sust Energ Rev **74** 938-948 (2017).

[2] J. Q. E, M. Pham, D. Zhao, Y. W. Deng, D. Le, W. Zuo, H. Zhu, T. Liu, Q. G. Peng, and Z. Q. Zhang, "Effect of different technologies on combustion and emissions of the diesel engine fueled with biodiesel: A review," Renew Sust Energ Rev **80** 620-647 (2017).

[3] M. Sui, Z. H. Zhu, F. S. Li, and H. Wang, "Effect of ferrocene as a combustion catalyst on the premixed combustion flame characteristics of Jatropha biodiesel," Combust Flame **259** (2024).

[4] X. L. Chen, Y. X. Shi, Y. X. Cai, J. F. Xie, Y. Q. Yang, D. L. Hou, and Y. S. Fan, "Effect of non-thermal plasma injection flow rate on diesel particulate filter regeneration at room temperature," Carbon Lett **34** 1075-1089 (2024).

[5] Y. Gao, J. Deng, C. W. Li, F. L. Dang, Z. Liao, Z. J. Wu, and L. G. Li, "Experimental study of the spray characteristics of biodiesel based on inedible oil," Biotechnol Adv **27**(5), 616-624 (2009).

[6] T. Pachiannan, W. J. Zhong, T. M. Xuan, B. Li, Z. X. He, Q. Wang, and X. Yu, "Simultaneous study on spray liquid length, ignition and combustion characteristics of diesel and hydrogenated catalytic biodiesel in a constant volume combustion chamber," Renew Energ **140** 761-771 (2019).

[7] J. X. Guo, M. N. Jiang, X. L. Li, M. U. Farid, B. J. Deka, B. P. Zhang, J. W. Sun, Z. K. Wang, C. H. Yi, P. W. Wong, S. Jeong, B. Gu, and A. K. An, "Springtail-inspired omniphobic slippery membrane with nano-concave re-entrant structures for membrane distillation," Nat Commun **15**(1), 7750 (2024).

[8] J. X. Guo, D. Y. S. Yan, F. L. Y. Lam, B. J. Deka, X. C. Lv, Y. H. Ng, and A. K. An, "Self-cleaning BiOBr/Ag photocatalytic membrane for membrane regeneration under visible light in membrane distillation," Chem Eng J **378** 122137 (2019).

[9] N. G. Chen, and Y. H. Gan, "Enhanced evaporation and heat transfer of sessile droplets via coupling electric field and temperature field," Chem Eng J **498** 155259 (2024).

[10] G. Chen, Z. Y. Dai, S. B. Li, Y. F. Huang, Y. Xu, J. C. She, and B. P. Zhou, "Magnetically Responsive Film Decorated with Microcilia for Robust and Controllable Manipulation of Droplets," Acs Appl Mater Inter **13**(1), 1754-1765 (2021).

[11] Y. X. Zhang, S. J. Jiang, Y. L. Hu, T. Wu, Y. Y. Zhang, H. Z. Li, A. Li, Y. C. Zhang, H. Wu, Y. L. Ding, E. R. Li, J. W. Li, D. Wu, Y. L. Song, and J. R. Chu, "Reconfigurable Magnetic Liquid Metal Robot for High-Performance Droplet Manipulation," Nano Lett **22**(7), 2923-2933 (2022).

[12] W. S. Yan, C. P. Zhao, W. Y. Luo, W. Y. Zhang, X. Li, and D. Liu, "Optically Guided Pyroelectric Manipulation of Water Droplet on a Superhydrophobic Surface," Acs Appl Mater Inter **13**(19), 23181-23190 (2021).

[13] W. Li, X. Tang, and L. Q. Wang, "Photopyroelectric microfluidics," Sci Adv **6**(38), eabc1693 (2020).

[14] L. Rayleigh, "On The Instability Of Jets," Proc. London Math. Soc **S1-10** 4-13 (1878).

[15] R. H. Magarvey, and L. E. Outhouse, "Note on the break-up of a charged liquid jet," J. Fluid Mech. **13**(01), 151-157 (1962).

[16] Y. Guan, S. Wu, M. D. Wang, Y. Tian, C. P. Yu, W. X. Lai, and Y. A. Huang, "Numerical investigation of high-frequency pulsating electrohydrodynamic jet at low electric Bond numbers," Phys Fluids **34**(1), 012001 (2022).

[17] Z. T. Wang, Q. Kong, B. Li, J. M. Tian, K. Yu, and J. F. Wang, "Electrohydrodynamic instability and disintegration of low viscous liquid jet," Phys Fluids **34**(12), 123301 (2022).

[18] K. K. Aminjan, M. Sedaghat, M. Heidari, M. Khashehchi, K. Mohammadzadeh, M. Salahinezhad, and R. Bina, "Numerical investigation of the impact of fuel temperature on spray characteristics in a pressure-swirl atomizer with spiral path," Exp Comput Multi Flo **6**(4), 428-445 (2024).

[19] Q. S. Wang, Z. T. Wang, Y. Jiang, M., and S. Q. Yang, "Experimental study of electro-spraying modes of deionized water in atmospheric environment," Exp Comput Multi Flo **3**(1), 38-46 (2021).

[20] D. B. Wang, J. F. Wang, D. R. Wang, and Q. S. Bi, "Electrically driven coalescence of charged conical droplet in non-uniform electric field," Chem Eng Sci **292** 119977 (2024).

[21] J. Li, N. S. Ha, T. Liu, R. M. van Dam, and C. J. Kim, "Ionic-surfactant-mediated electro-dewetting for digital microfluidics," Nature **572**(7770), 507-510 (2019).

[22] J. H. Nie, Z. W. Ren, J. J. Shao, C. R. Deng, and W. L. Zhong, "Self-Powered Microfluidic Transport System Based on Triboelectric Nanogenerator and Electrowetting Technique," Acs Nano **12**(2), 1491-1499 (2018).

[23] L. Zheng, Y. L. Wu, X. Y. Chen, A. F. Yu, L. Xu, Y. S. Liu, H. X. Li, and Z. L. Wang, "Self-Powered Electrostatic Actuation Systems for Manipulating the Movement of both Microfluid and Solid Objects by Using Triboelectric Nanogenerator," Adv Funct Mater **27**(16), 1606408 (2017).

[24] N. G. Chen, Y. H. Gan, D. F. Shi, Y. L. Luo, and Z. W. Jiang, "Experimental investigation on the electrospray counterflow flame in a small combustor with a porous media as the grounding electrode," Energy **284** 128611 (2023).

[25] N. G. Chen, Y. H. Gan, Y. L. Luo, and Z. W. Jiang, "A review on the technology development and fundamental research of electrospray combustion of liquid fuel at small-scale," Fuel Process Technol **234** 107342 (2022).

[26] H. H. Xia, B. Y. Yu, K. Chang, X. Y. Zhao, and W. W. Deng, "Shaping electrospray deposition profile by a quadrupole: From circular to elliptical patterns," J Aerosol Sci **154** 105739 (2021).

[27] Z. W. Jiang, Y. H. Gan, and Y. L. Shi, "An improved model for prediction of the cone-jet formation in electrospray with the effect of space charge," J Aerosol Sci **139** 105463 (2020).

[28] M. Kass, B. Kaul, B. Armstrong, J. Szybist, and V. Lobodin, "Stability, rheological and combustion properties of biodiesel blends with a very-low sulfur fuel oil (VLSFO)," Fuel **316** 123365 (2022).

[29] Z. W. Jiang, Y. H. Gan, Y. G. Ju, J. L. Liang, and Y. Zhou, "Experimental study on the electrospray and combustion characteristics of biodiesel-ethanol blends in a meso-scale combustor," Energy **179** 843-849 (2019).

[30] L. Zuo, J. F. Wang, D. Q. Mei, D. B. Wang, W. Zhang, H. J. Xu, J. Yao, and T. Y. Zhao, "Atomization and combustion characteristics of a biodiesel-ethanol fuel droplet in a uniform DC electric field," Phys Fluids **35**(1), 013303 (2023).

[31] M. Zaharin, S. M., N. Abdullah, R., G. Najafi, H. Sharudin, and T. Yusaf, "Effects of physicochemical properties of biodiesel fuel blends with alcohol on diesel engine performance and exhaust emissions: A review," Renewable and Sustainable Energy Reviews **79** 475-493 (2017).

[32] Z. T. Wang, Y. Z. Chen, J. Y. Xue, B. Li, J. Wang, and Q. M. Dong, "Electrospray modes of liquids in electrohydrodynamic atomization: A review," Phys Fluids **36**(11), (2024).

[33] C. Kwon, U. P. Padhi, P. Kumar, D. Lim, S. Choe, K. Kwon, and J. J. Yoh, "A novel annular slit-type emitter developed for multi-jet electrospray propulsion," Phys Fluids **36**(2), 27128 (2024).

[34] O. Yogi, T. Kawakami, and A. Mizuno, "Properties of droplet formation made by cone jet using a novel capillary with an external electrode," J Electrostat **64**(7-9), 634-638 (2006).

[35] Y. H. Gan, N. G. Chen, X. H. Zheng, D. F. Shi, Z. W. Jiang, S. R. Song, and Y. L. Shi, "Electric field and spraying characteristics of electrospray using concave ground electrode," J Electrostat **115** (2022).

[36] Z. T. Wang, L. Xia, and S. Q. Zhan, "Experimental study on electrohydrodynamics (EHD) spraying of ethanol with double-capillary," Applied Thermal Engineering **120** 474-483 (2017).

[37] J. Zhang, H. Z. He, and G. X. Huang, "Dynamic characteristics of charged droplets in an electrostatic spraying process with twin capillaries," Chinese J Chem Eng **26**(12), 2403-2411 (2018).

[38] H. Zhu, Y. Huang, D. Peng, Z. Liao, H. Lu, and Q. Yang, "Droplet formation regime and size prediction in substantial mass transfer systems," Chem Eng J **496** 154119 (2024).

[39] Y. H. Gan, Y. Tong, Y. G. Ju, X. Zhang, H. G. Li, and X. W. Chen, "Experimental study on electro-spraying and combustion characteristics in meso-scale combustors," Energ Convers Manage **131** 10-17 (2017).

[40] M. Cloupeau., and B. Prunet-Foch, "Electrohydrodynamic spraying functioning modes: A critical review," J. Aerosol Sci **25**(6), 1021-1036 (1994).

[41] H. J. Xu, J. F. Wang, J. M. Tian, B. Li, J. Yao, L. Zuo, Y. Zhang, and T. Y. Zhao, "Electrohydrodynamic disintegration of dielectric fluid blended with ethanol," Phys Fluids **33**(6), 062107 (2021).

[42] W. Zhang, J. F. Wang, W. H. Hu, H. L. Liu, B. Li, and K. Yu, "Enhancement of electric field on bubble dispersion characteristics in leaky-dielectric liquid medium," Int J Multiphas Flow **142** 103743 (2021).

[43] J. S. Shrimpton, and Y. Laoonual, "Dynamics of electrically charged transient evaporating sprays," Int J Numer Meth Eng **67**(8), 1063-1081 (2006).

[44] P. Di Marco, R. Kurimoto, G. Saccone, K. Hayashi, and A. Tomiyama, "Bubble shape under the action of electric forces," Experimental Thermal and Fluid Science **49** 160-168 (2013).

[45] W. Zhang, J. F. Wang, S. J. Yang, B. Li, K. Yu, D. B. Wang, P. Yongphet, and H. J. Xu, "Dynamics of bubble formation on submerged capillaries in a non-uniform direct current electric field," Colloid Surface A **606** 125512 (2020).

[46] L. Rayleigh, "On the equilibrium of liquid conducting masses charged with electricity," Philosophical Magazine **14** 184-186 (1882).

[47] Y. P. Huo, J. F. Wang, Z. W. Zuo, and Y. J. Fan, "Visualization of the evolution of charged droplet formation and jet transition in electrostatic atomization," Phys Fluids **27**(11), 114105 (2015).

[48] N. G. Chen, Y. H. Gan, and Y. L. Shi, "Enhanced controllability of droplet evaporation via DC electric field," Chem Eng J **479** 147488 (2024).

[49] W. Zhang, J. F. Wang, B. Li, K. Yu, D. B. Wang, P. Yongphet, H. J. Xu, and J. Yao, "Experimental investigation on bubble coalescence regimes under non-uniform electric field," Chem Eng J **417** 127982 (2021).